CLIMATOLOGY

Arctic Ocean Amplification in a warming climate in CMIP6 models

Qi Shu[1,2,3], Qiang Wang[4]*, Marius Årthun[5], Shizhu Wang[1,2,3], Zhenya Song[1,2,3], Min Zhang[1,2,3], Fangli Qiao[1,2,3]*

Arctic near-surface air temperature warms much faster than the global average, a phenomenon known as Arctic Amplification. The change of the underlying Arctic Ocean could influence climate through its interaction with sea ice, atmosphere, and the global ocean, but it is less well understood. Here, we show that the upper 2000 m of the Arctic Ocean warms at 2.3 times the global mean rate within this depth range averaged over the 21st century in the Coupled Model Intercomparison Project Phase 6 Shared Socioeconomic Pathway 585 scenario. We call this phenomenon the "Arctic Ocean Amplification." The amplified Arctic Ocean warming can be attributed to a substantial increase in poleward ocean heat transport, which will continue outweighing sea surface heat loss in the future. Arctic Amplification of both the atmosphere and ocean indicates that the Arctic as a whole is one of Earth's regions most susceptible to climate change.

INTRODUCTION

As the northernmost region of Earth, the Arctic has been experiencing the most notable climate change over the past few decades. Arctic sea ice concentration and extent have declined markedly in all regions and seasons in the satellite era (*1*, *2*). The recent Arctic sea ice extent reductions in September are unprecedented over at least the past 1000 years (*3*, *4*). Moreover, Arctic sea ice volume and the percentage of multiyear sea ice have decreased markedly (*5*, *6*). It is likely that the Arctic Ocean will experience ice-free summers before 2050 (*7*, *8*).

Both observations and model results show a rapid warming of the Arctic troposphere since the 1990s, with the maximum warming rate near the surface in autumn and winter (*9*–*11*). The rise of near-surface air temperature in the Arctic is more than twice that of the global average (*9*–*12*), which is a phenomenon known as "Arctic Amplification" (AA). It is believed that AA is caused by both local and remote forcing mechanisms (*11*, *13*), including the sea ice albedo feedback (*9*, *14*, *15*), lapse rate and Planck feedback (*14*, *16*), ocean heat capacitor mechanism (*17*), and atmospheric and ocean heat transport from lower latitudes into the Arctic (*18*, *19*).

In comparison with the observations of Arctic sea ice and atmosphere, data of the Arctic Ocean are much sparser. Warming signals in the ocean are nevertheless detected based on limited observations and model simulations (*20*–*26*). Prominent Arctic Ocean warming has been found in the Barents Sea and Arctic Atlantic water (AW) layer (~150 to 900 m). The Barents Sea temperature increased by 1.74°C during the period 1965–2015 (*25*). The observed linear trend of spatially averaged AW layer maximum temperature in the Arctic Basin is 0.21°C ± 0.04°C per decade over the historical period since 1950, and the warming has been pronounced since the 1990s and suspected to be mainly caused by anomalous heat advection from the North Atlantic (*27*, *28*). The Arctic Ocean change associated with advection of anomalous AW heat, mass, and tracers is called Arctic Atlantification (*28*, *29*). Arctic Pacification, the counterpart of Atlantification associated with Pacific water inflow through Bering Strait, has also been observed and evident in strengthening the upper ocean warming in the Canada Basin (*28*, *30*). Changes in air-sea heat flux along the Atlantic and Pacific water inflow pathways can substantially influence the process of Arctic borealization (Atlantification and Pacification) downstream in the Arctic Ocean (*31*–*33*). In the process of the Arctic borealization, sea surface heat release decreases in the upstream ice-free region and more ocean heat is left in the ocean, thus leading to enhanced ocean warming and sea surface heat release in downstream regions of the Arctic Ocean (*33*).

Climate model projections show that Arctic Atlantification and Pacification will continue under scenarios of global warming (*28*, *33*, *34*), indicating that more ocean heat will be transported into the Arctic Ocean, causing further Arctic Ocean warming in the future. On the other hand, owing to the rapid Arctic sea ice decline and the halocline weakening in the regions influenced by AW inflow in a warming climate, the Arctic Ocean will release more heat to the atmosphere (*33*, *35*). The future changes in the Arctic Ocean temperature will depend on the evolution of these two opposing contributions. AA, much stronger Arctic atmosphere warming than the global mean, has occurred and will continue in the future warming climate (*36*). The occurrence of Arctic Ocean Amplification (AOA), much stronger Arctic Ocean warming than the global mean, has not been identified on the basis of observations so far because ocean observations below the surface are relatively sparse.

In this study, we analyzed 20 climate model historical simulations and Shared Socioeconomic Pathway 585 (SSP585) scenario projections of the Coupled Model Intercomparison Project Phase 6 (CMIP6). Our results demonstrate that AOA has most likely started already and will continue with climate warming. The Arctic Ocean warming will have an increasing rate, which can be attributed to the fact that the enhancement of ocean heat convergence into the Arctic Ocean will be greater than the increase of Arctic Ocean surface heat loss.

[1]First Institute of Oceanography and Key Laboratory of Marine Science and Numerical Modeling, Ministry of Natural Resources, Qingdao, China. [2]Laboratory for Regional Oceanography and Numerical Modeling, Qingdao National Laboratory for Marine Science and Technology, Qingdao, China. [3]Shandong Key Laboratory of Marine Science and Numerical Modeling, Qingdao, China. [4]Alfred Wegener Institute, Helmholtz Centre for Polar and Marine Research (AWI), Bremerhaven, Germany. [5]Geophysical Institute, University of Bergen and Bjerknes Centre for Climate Research, Bergen, Norway.
*Corresponding author. Email: qiaofl@fio.org.cn (F.Q.); qiang.wang@awi.de (Q.W.)

RESULTS

Arctic Ocean Amplification

Both observation-based data [EN4; (*37*)] and CMIP6 simulations indicate noticeable ocean warming during the past few decades, especially in the Northern Hemisphere (Fig. 1, A and B). The ocean warming will become notably large at the end of the 21st century in the SSP585 scenario (Fig. 1C). It mainly occurs in the upper 2000 m, with more rapid warming in water mass subduction regions and the Arctic Ocean (Figs. 1, A to C, and 2A). In comparison with the global average, the Arctic Ocean exhibits much larger temperature increase when we consider the upper 700 m, upper 2000 m, or the whole water column (Fig. 1, D to F, and Table 1). We call this phenomenon AOA. Unlike AA in the atmosphere that has the most notable amplification signal near the surface, AOA is characterized by the greatest warming in the Arctic AW layer located at intermediate depths (~150 to 900 m; Fig. 1C). The Arctic AW layer will warm by about 2.89°C until 2081–2100 relative to 1981–2000, standing out from the warming in the same depth range at other latitudes (Fig. 1C and Table 1). The warming rate (temperature time derivative) will increase throughout the 21st century for both the Arctic Ocean and the global ocean (Fig. 1, G and H).

We define the AOA factor as the ratio of the warming rate of the Arctic Ocean to that of the global ocean. The natural variability in temperature is removed before computing the warming rate (see Materials and Methods). The AOA factor indicates that the Arctic Ocean will warm at a rate approximately 1.0 to 3.0 times that of the global ocean average, depending on the depth ranges considered (Fig. 1I). For the upper 150 m, the Arctic Ocean has a warming rate

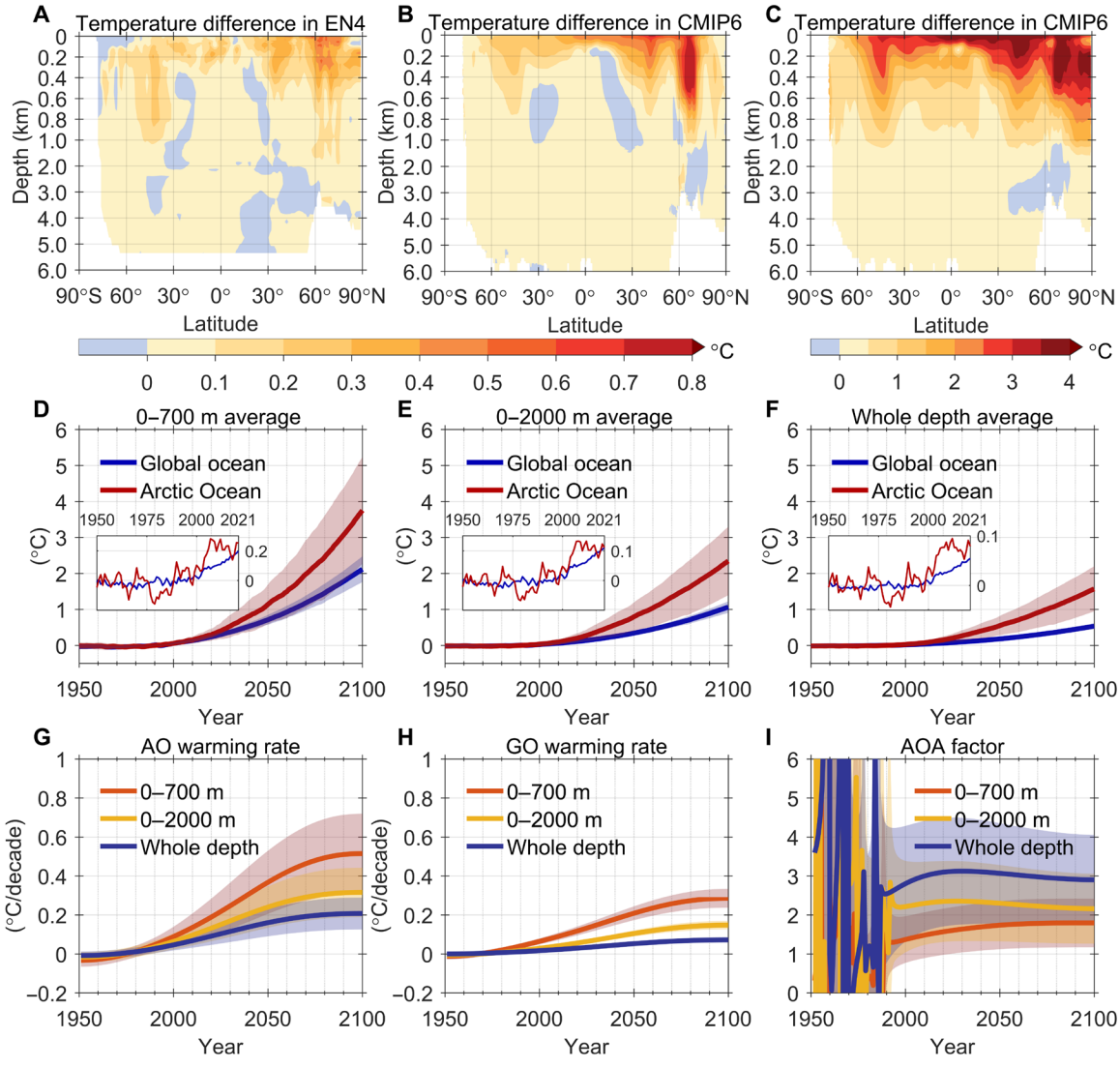

Fig. 1. Arctic Ocean Amplification. Difference in zonal mean ocean temperature between 2001–2020 and 1981–2000 based on (**A**) EN4 dataset and (**B**) CMIP6. (**C**) Difference in zonal mean ocean temperature between 2081–2100 and 1981–2000 in CMIP6. Global mean and Arctic Ocean mean changes in ocean temperature for (**D**) upper 700 m, (**E**) upper 2000 m, and (**F**) the whole depth range relative to the 1981–2000 mean. (**G**) Arctic Ocean (AO) and (**H**) global ocean (GO) forced warming rate. (**I**) AOA factor, which is the ratio of the forced warming rate of the Arctic Ocean to that of the global ocean. The multimodel means based on CMIP6 simulations and projections under scenario SSP585 are shown in (B) to (I). Shading in (D) to (I) shows the range of one SD of the CMIP6 models. The inserted panels in (D) to (F) are the results during 1950–2021 based on the EN4 dataset. Note that the colorbar for (A) and (B) is different from that for (C).

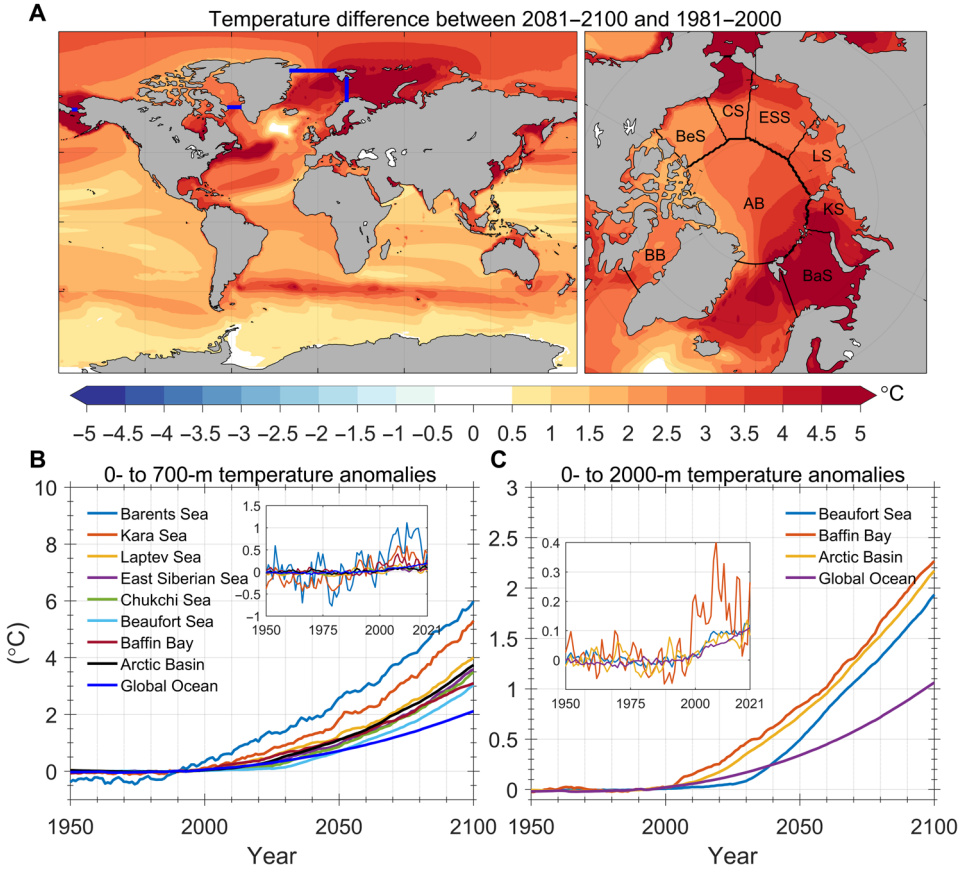

Fig. 2. Regional ocean warming. (**A**) Difference of ocean temperature averaged over upper 700 m between 2081–2100 and 1981–2000. BaS, KS, LS, ESS, CS, BeS, BB, and AB represent the Barents Sea, Kara Sea, Laptev Sea, East Siberian Sea, Chukchi Sea, Beaufort Sea, Baffin Bay, and Arctic deep basin, respectively. Blue lines in (A) indicate the four main gateways [i.e., the Bering Strait, Barents Sea Opening (BSO), Fram Strait, and Davis Strait] of the Arctic Ocean. Regional and global ocean temperature anomalies relative to 1981–2000 for the (**B**) upper 700 m and (**C**) upper 2000 m, respectively. The inserted panels in (B) and (C) are the results during 1950–2021 based on the EN4 dataset. For the regions with water depth less than 700 m, the average was taken over the full-depth range.

Table 1. Changes in Arctic Ocean and global ocean mean temperature for 2081–2100 relative to 1981–2000 and AOAF. The considered depth ranges are indicated in the first column. Multimodel means and ±σ (1 SD) are given here. AOAF, AOA factor.

Depth ranges (m)	Global Ocean (°C)	Arctic Ocean (°C)	AOAF
0–150	2.86 ± 0.58	3.15 ± 1.55 (polar surface water)	1.0 ± 0.4
0–300	2.46 ± 0.50	3.26 ± 1.50	1.3 ± 0.4
0–700	1.80 ± 0.31	3.11 ± 1.36	1.7 ± 0.6
150–900	1.27 ± 0.21	2.89 ± 1.25 (AW)	2.3 ± 0.9
0–2000	0.90 ± 0.14	2.00 ± 0.88	2.3 ± 1.0
900–bottom	0.15 ± 0.03	0.43 ± 0.26 (deep/bottom waters)	3.2 ± 2.1
Full depth	0.45 ± 0.06	1.34 ± 0.58	3.0 ± 1.3

similar to the global ocean average (Table 1). However, for the upper 700 m, the AOA factor averaged over the whole 21st century is about 1.7 ± 0.6 (multimodel means ± 1 SD; Fig. 1I and Table 1), with volume-weighted ocean temperature changes of 3.11°C ± 1.36°C and 1.80°C ± 0.31°C between the long-term future (2081–2100) and the period of 1981–2000 in the Arctic Ocean and the global ocean, respectively (Table 1). For the upper 2000 m, the mean AOA factor is 2.3 ± 1.0 (Fig. 1I and Table 1), and the temperature changes are 2.00°C ± 0.88°C and 0.90°C ± 0.14°C in the Arctic Ocean and the global ocean, respectively (Table 1). For the whole depth of the ocean, the mean AOA factor is even larger (3.0 ± 1.3). This is mainly because the percentage of the deep ocean volume in the Arctic Ocean is smaller than that of the global ocean, and the temperature changes below 2000 m depth is small in all latitudes (Fig. 1C). The AOA factor for the upper 2000 m has a peak at around 2020, while the AOA factor for the upper 700 m will increase until about 2080 (Fig. 1I). On the seasonal time scale, the AOA factor has negligible variability in the AW layer (fig. S1). Therefore, both the seasonal variability and the future change of the AOA factor are different from the AA, which has a seasonal cycle and will drop in the future (*38*).

Both the warming rates for the Arctic Ocean and the global ocean were relatively low in the past (before 2020) compared with the projected future warming rates (Fig. 1, G and H), but the AOA already emerged in the mid-1990s (Fig. 1I), after which the AOA factors of all the CMIP6 models remain larger than one. The time of emergence (ToE) of AOA based on the Community Earth System Model (CESM) large ensemble simulations is 1985 ± 13 (fig. S2). Therefore, the CMIP6 models and the CESM large ensemble simulations

consistently show that the AOA already emerged in these model simulations at the end of the past century.

Arctic Ocean warming will be spatially nonuniform (Fig. 2 and table S1). The Barents Sea will have the greatest temperature increase in the Arctic Ocean, followed by the Kara Sea. Sea water temperature will warm by 5.17°C ± 2.00°C and 4.40°C ± 1.96°C in the Barents and Kara seas, respectively, for 2081–2100 relative to 1981–2000 (table S1). The strong warming in the Barents, Kara, and Chukchi seas reflects the impact of the warm Atlantic and Pacific waters. Excluding the Arctic shelf seas, which are typically shallower than 100 m except for the Barents Sea, does not change the fact that the Arctic Ocean has stronger warming than the global mean. For example, the warming averaged over the upper 2000 m will be 0.90°C ± 0.14°C and 1.86°C ± 0.87°C for the global ocean and the central Arctic Basin, respectively, indicating an amplification factor of 2.1 ± 1.0 (table S1). It is only slightly lower than the AOA factor of 2.3 ± 0.9 for the upper 2000 m of the whole Arctic Ocean (Table 1). The Beaufort Sea will have the lowest warming in the Arctic Ocean. Nevertheless, the temperature change in the Beaufort Sea of 1.63°C ± 0.87°C averaged over the upper 2000 m is still much larger than the global average.

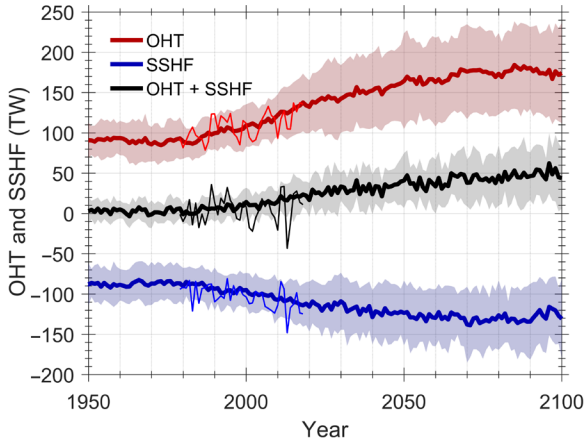

Fig. 3. Arctic Ocean heat budget analysis. Time series of net ocean heat transport (OHT) (red) summed over the four Arctic gateways (i.e., the Bering Strait, BSO, Fram Strait, and Davis Strait), sea surface heat flux (SSHF) (blue) averaged over the Arctic Ocean, and the sum of ocean heat transport and sea surface heat flux (black). Shading shows the range of 1 SD of the CMIP6 models. Poleward ocean heat transport is positive. Upward sea surface heat flux (heat loss) is negative. Thin lines are results based on the ORAS5 ocean reanalysis dataset.

Drivers of AOA

The evolution of Arctic Ocean temperature is determined by changes in the net ocean heat transport through four gateways [i.e., Bering Strait, Barents Sea Opening (BSO), Fram Strait, and Davis Strait; geometric locations shown in fig. S3] and sea surface heat flux over the Arctic Ocean (*39*). For the net ocean heat transport into the Arctic Ocean, both observations and historical simulations show positive trends over the past 30 years (*24*, *40*–*44*). CMIP6 climate models are able to reproduce the historical positive trend, and their projections indicate that this positive trend is likely to continue until approximately 2070 under scenario SSP585, after which it will become stable without further substantial change (Fig. 3). For sea surface heat flux, increased heat loss from the Arctic Ocean to the atmosphere owing to sea ice decline has been reported (*27*, *33*, *35*). The CMIP6 historical simulations and projections under scenario SSP585 show that the increase in Arctic Ocean surface heat release has started since about the 1990s and will continue in the future, reaching a peak at around 2070, followed by a slight decrease (Fig. 3).

Although both the net ocean heat transport into the Arctic Ocean and Arctic Ocean surface heat release will increase until around 2070, the net heat gain of the Arctic Ocean (black line in Fig. 3) is projected to increase continuously until that time because the increase in ocean heat transport is larger than the increase in sea surface heat loss. The upward trend in the net heat gain explains the accelerating warming of the Arctic Ocean before 2070 (Fig. 1F). After 2070, the Arctic Ocean net heat gain starts to level off (Fig. 3), as also shown by the warming rate of the Arctic Ocean (Fig. 1G). The warming rate of the Arctic Ocean, despite its slowdown after 2070, remains much larger than the global mean warming rate throughout the 21st century for different ocean depth ranges (Fig. 1, G and H), so the AOA is expected to remain persistent in a warming climate (Fig. 1I).

Overall, the net ocean heat transport outweighs the Arctic Ocean surface heat loss through the 21st century (Fig. 3), sustaining a substantial Arctic Ocean warming (fig. S4). Each individual CMIP6 model also consistently shows that the Arctic Ocean warming is driven by an increase in ocean heat transport through the Arctic gateways (fig. S5), while the previous CMIP5 simulations had large model uncertainties in this regard (*39*).

Evolution of ocean heat transport into the Arctic Ocean

To understand the evolution of net ocean heat transport into the Arctic Ocean, the heat transport through the four Arctic Ocean gateways associated with inflows and outflows was calculated separately (Fig. 4). It is projected that both the ocean heat import and export will increase continuously in the future (Fig. 4A). The net ocean heat transport will increase until 2070 because of the stronger increase in heat inflow transport than in heat outflow transport. However, the increase in heat outflow transport will accelerate with time and it will start to offset the increase in heat inflow transport starting from about 2070, thus causing the net ocean heat transport to stay at a semi-stationary level during 2070–2100 (Fig. 4A).

Ocean heat inflow will increase at all the four gateways, and the strongest increase is found at the BSO (Fig. 4, B to E). Ocean heat transport out of the Arctic Ocean will increase with time at the Fram and Davis Straits (Fig. 4, D and E), while the change in heat export through the Bering Strait and BSO will be negligible (Fig. 4, B and C). Therefore, it is the increasing ocean heat export through the Fram and Davis Straits that causes the net ocean heat transport into the Arctic Ocean to level off after 2070 (Fig. 4A). Different from the Davis Strait export, the warm water exported through the Fram Strait is from the Arctic deep basin, so the increasing ocean heat export through the Fram Strait directly limits the accumulation of ocean heat in the Arctic deep basin.

Ocean heat transport anomalies can be decomposed into temperature-driven, velocity-driven, and temperature and velocity joint-variability components (see Materials and Methods) (*44*). The temperature-driven and velocity-driven components for all four gateways will have the largest and smallest contributions to the heat transport anomalies, respectively (fig. S6). This indicates that the future increase in ocean heat supply to the Arctic Ocean can be mainly attributed to the ocean warming outside the Arctic Ocean rather than increases in ocean volume transport. Besides, the joint

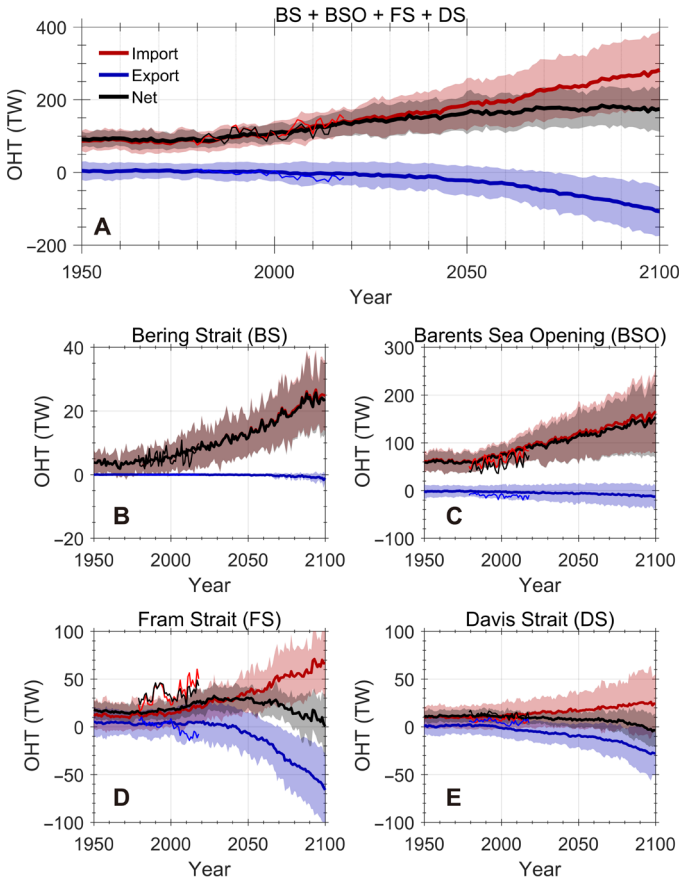

Fig. 4. Time series of ocean heat transport through the Arctic Ocean gateways. Time series of import (red), export (blue), and net (black) ocean heat transport through the Arctic Ocean gateways. Shading shows the range of 1 SD of the CMIP6 models. (**A**) Total ocean heat transport through the four gateways (i.e., the Bering Strait, BSO, Fram Strait, and Davis Strait). (**B** to **E**) The ocean heat transport through each individual gateway. Thin lines are results based on the ORAS5 ocean reanalysis dataset.

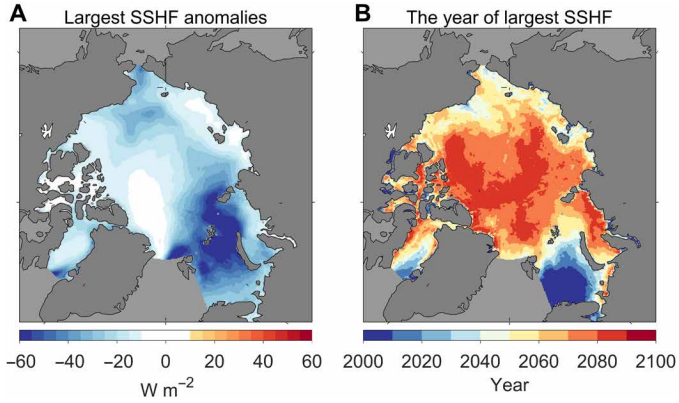

Fig. 5. Largest anomalies of annual mean sea surface heat release and the time of their occurrence. (**A**) Largest negative anomalies of annual mean sea surface heat flux and (**B**) year of their occurrence. Negative sea surface heat flux anomalies indicate enhanced ocean surface heat loss. The anomalies are referenced to the mean over the period 1981–2000.

variability of temperature and velocity at the BSO, Fram Strait, and Davis Strait will contribute to Arctic Ocean warming, whereas at the Bering Strait, it will have the opposite effect (fig. S6). The enlargement of the negative temperature-driven ocean heat transport anomalies at the Fram and Davis Straits can be explained by the warming trend in the outflow water from the Arctic Ocean (fig. S7).

Evolution of Arctic Ocean surface heat release

To understand the nonmonotonic changes in Arctic Ocean surface heat release (Fig. 3), the largest anomalies of the net sea surface heat release and the time of their occurrence in the Arctic Ocean are shown in Fig. 5. The largest net ocean heat release anomalies will occur in the northern Barents Sea, the Kara Sea, and the eastern part of the Eurasian Basin (Fig. 5 and fig. S8). Notable enhancement of AW heat transport into the Arctic Ocean through the BSO and Fram Strait will lead to rapid sea ice decline (*27*, *29*). This weakens the insulating effect of sea ice in air-sea interaction processes and, hence, increases sea surface heat release in the previously ice-covered regions (*29*, *33*). After reaching a maximum as these regions become ice-free, ocean surface heat release will gradually decrease (fig. S8) primarily because of the decrease in sensible heat flux owing to more rapid warming of the near-surface atmosphere in comparison with sea surface warming (*33*). The increase in ocean heat transport through the Bering Strait and Davis Strait will also lead to similar changes in the sea surface heat flux in the Chukchi Sea, Canada Basin, and Baffin Bay, but the changes in these regions will be smaller (Fig. 5 and fig. S8). The sea surface heat flux anomalies in Fig. 5A roughly depict the pathways of Atlantic and Pacific water inflows, which manifests that the Arctic Atlantification and Pacification will be strengthened in the future warming climate and have an increasing impact on Arctic sea ice decline (*33*, *45*).

Figure 5 shows that the net sea surface heat release in most of the Arctic Ocean is projected to reach maximum before 2080 under scenario SSP585. Subsequently, the sea surface heat flux averaged over the Arctic Ocean will present a positive trend (less heat loss; Fig. 3), primarily because of the notable positive trends during 2071–2100 in the Barents Sea, Kara Sea, Chukchi Sea, and Baffin Bay (fig. S8).

Effects of Arctic Ocean warming on the ocean density and halocline base depth

In addition to the notable warming, the Arctic Ocean will also store more fresh water in a warming climate (*46*, *47*). Consequently, the potential density of the Arctic Ocean will decrease substantially at both the upper and intermediate depths (in the upper 1500 m; Fig. 6, A and B). The potential density decrease is mainly due to the reduction in salinity in the upper 100 m of the Eurasian Basin and in the upper 150 m of the Amerasian Basin, while at the intermediate depth, it can be attributed to both the ocean freshening and warming. The warming in the Eurasian Basin is greater than that in the Amerasian Basin (Fig. 2A), so the effect of ocean warming on the potential density is larger in the Eurasian Basin (Fig. 6, A and B).

The March surface mixed layer depth is projected to increase in the Eurasian Basin and remain relatively stable in the Amerasian Basin (Fig. 6, C and D). The increase in surface buoyancy loss due to enhanced surface heat loss (Fig. 5A) and the possible increase in brine rejection in a warming climate (*48*) can explain the deepening of the mixed layer in the Eurasian Basin. The vertical gradient of the potential density, the stratification, in the upper 150 m of the Amerasian Basin becomes considerably stronger in the warming

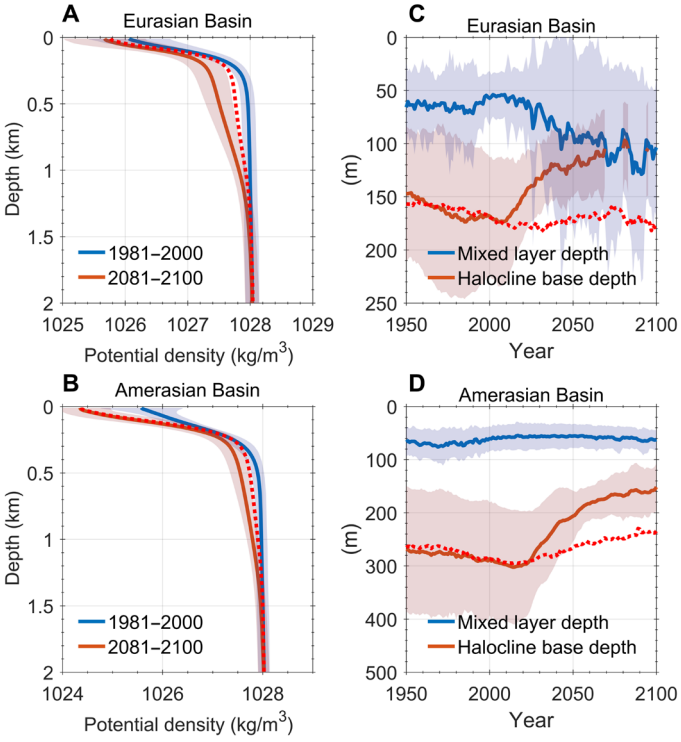

Fig. 6. Potential density, surface mixed layer depth, and halocline base depth in winter in the two Arctic basins. March potential density for the periods of 1981–2000 (blue solid lines) and 2081–2100 (red solid lines) in the (**A**) Eurasian and (**B**) Amerasian basins. Red dotted lines in (A) and (B) are based on salinity during 2081–2100 and potential temperature during 1981–2000. March mixed layer and halocline base depth in the (**C**) Eurasian and (**D**) Amerasian basins. Red dotted lines in (C) and (D) are halocline base depth calculated on the basis of variable salinity but fixed potential temperature of the 1981–2000 mean. The differences between the red solid lines and red dotted lines indicate the impacts of Arctic Ocean warming. Shading shows the range of 1 SD of the CMIP6 models.

climate (Fig. 6B), which can counterbalance the effect of surface buoyancy loss and thus maintains a stable mixed layer depth (Fig. 6D).

The Arctic halocline insulates sea ice and the mixed layer from the underlying warm AW layer (*49*). The halocline base, which defines the transition from halocline to thermocline, was observed to become shallow in the eastern Eurasian Basin in the past decade (*50*). It will continue to shoal in both the Arctic basins in a warming climate (Fig. 6, C and D). Averaged over the Eurasian Basin, the halocline base will reach the mixed layer lower boundary starting from about 2070 due to the deepening of the mixed layer and shoaling of the halocline base. The shoaling of the halocline base will facilitate the ocean heat in the AW layer to reduce sea ice cover and increase sea surface heat loss in winter as shown in Fig. 5A. The shoaling of the halocline base is mainly due to the ocean warming in the Eurasian Basin (Fig. 6C). Therefore, the ocean warming not only increases the available ocean heat but also weakens the halocline through reducing ocean density. In the Amerasian Basin, the halocline base will rise because of both the ocean warming and freshening in a warming climate, but, averaged over the basin, it will not reach the mixed layer lower boundary within the 21st century (Fig. 6D).

DISCUSSION

The Arctic Ocean is and will continue to be warming much faster than the global ocean average in a warming climate, a phenomenon that we call AOA. The AOA features the strongest Arctic Ocean warming at the intermediate depth where the AW layer locates, which can be attributed to enhanced ocean heat import through the BSO and Fram Strait. Our heat budget analysis indicates that the increase in the net ocean heat transport into the Arctic Ocean, despite being partially offset by the increase in the net surface heat loss, will drive an accelerating warming in the Arctic Ocean in the coming decades. Therefore, the AOA is largely a fingerprint of Arctic Atlantification, a process of anomalous ocean heat advection from the North Atlantic to the Arctic Ocean.

Our analysis indicates that the future increase in ocean heat transport into the Arctic Ocean is mainly due to ocean warming in the inflow water, not the increase in the ocean volume transport. The warming of the AW in the Nordic Seas is indeed pronounced in the future (Fig. 2A). It can be attributed to a reduction in sea surface heat loss and an increase in ocean heat transport from the subpolar North Atlantic (SPNA), and these two factors have similar contributions (fig. S9). The weakening of the Atlantic Meridional Overturning Circulation in a warming climate can slow down the ocean warming in the SPNA (*51*), but the net ocean heat transport into the Nordic Seas will keep increasing (fig. S9) because the local ocean circulation in the SPNA plays an important role in influencing the poleward ocean heat transport (*52*, *53*). The increase in ocean heat inflow from the Pacific associated with Arctic Pacification also contributes to the Arctic Ocean warming, but its impact can be mainly on the upper ocean because of the low density of fresh Pacific Water.

Ocean heat export from the Arctic Ocean to the North Atlantic will increase as a result of increasing temperature in the export water at the Fram and Davis straits (fig. S7). This will cause the net ocean heat supply to the Arctic Ocean to level off after 2070 in the CMIP6 SSP585 scenario. Therefore, the ocean heat export will become an important heat budget term of the Arctic Ocean in the future, although it was not so in the past. Owing to the shoaling of the AW layer, weakening of the Arctic halocline, and deepening of the mixed layer, the Arctic Ocean surface heat loss will increase in a warming climate, especially along the pathways of Atlantic and Pacific water inflow. This will contribute to the near-surface air warming and AA. The more rapid warming of the Arctic atmosphere in areas of open seas, a manifestation of the AA, tends to reduce the ocean surface heat loss (*24*, *33*). This causes the total surface heat loss to decrease slowly after reaching the maximum in about 2070. The changes in both the ocean heat transport and surface heat loss after 2070 together cause the rate of the heat gain of the Arctic Ocean to stay at a relatively stable level. As a consequence, the Arctic Ocean will continue to warm up until the end of the 21st century.

The AOA has emerged already and will continue in the warming climate. This indicates that the Arctic Ocean is one of the oceans most susceptible to climate change. The Barents Sea is the Arctic area that first exhibits signs of strong and accelerating warming (Fig. 2B). The associated notable influence on marine ecosystems and sea ice decline has already been evident (*23*–*25*, *29*, *54*). Warming of the Chukchi Sea and the AW layer in the Arctic Ocean, which also has strong implications on marine ecosystems and sea ice decline, has also been reported (*21*, *27*, *28*, *55*). The amplified Arctic Ocean warming in the CMIP6 SSP585 scenario implies that the physical environment and marine life in the Arctic Ocean will

face marked changes in the future unless climate change can be timely alleviated.

Because of the rapid warming and notable freshening in the Arctic Ocean in a warming climate, the local steric (thermosteric and halosteric) sea level in the Arctic Basin will also rise faster than the global mean. On the basis of our estimate, the steric sea level in the Arctic Basin during 2081–2100 will rise by 0.48 ± 0.16 m relative to 1981–2000, while the global mean steric sea level will rise by 0.30 ± 0.06 m. Ocean heat uptake has strong impacts on the spatial pattern of atmosphere warming (*56*). Considering the relatively small volume of the Arctic Ocean, which accounts for about 1.4% of the global ocean volume, the rapid warming in the Arctic Ocean makes little direct contribution to the global heat uptake. However, the changes in Arctic Ocean surface heat flux associated with the increase in ocean heat transport and Arctic Ocean warming can directly enhance the regional atmosphere warming and AA. Furthermore, the local changes in the Arctic Ocean may have potential impacts on ocean and atmosphere circulations at lower latitudes through both ocean export and air-sea interactions (*57*–*59*), which requires sustained observations and improved understanding.

MATERIALS AND METHODS

Terminology

In this study, "Arctic Ocean" refers to the Arctic Basin (Eurasian and Amerasian basins) and its surrounding shelf seas, including the Barents, Kara, Laptev, East Siberian, Chukchi, and Beaufort seas, as well as Baffin Bay (fig. S3).

Dataset

This study used historical simulations and projections based on 20 CMIP6-coupled models (table S2): ACCESS-CM2, ACCESS-ESM1-5, AWI-CM-1-1-MR, CESM2-WACCM, CESM2, CMCC-CM2-SR5, CNRM-CM6-1-HR, CNRM-CM6-1, CNRM-ESM2-1, CanESM5-CanOE, CanESM5, EC-Earth3-Veg, EC-Earth3, FIO-ESM-2-0, GFDL-CM4, HadGEM3-GC31-LL, IPSL-CM6A-LR, NorESM2-LM, NorESM2-MM, and UKESM1-0-LL. The simulations for 1950–2014 and projections for 2015–2100 are based on CMIP6 historical and scenario experiments, respectively. The CMIP6 projections for 2015–2100 are driven by external forcings under the SSP framework (*60*). The projections used in this study are based on scenario SSP585, which is characterized by rapid and fossil-fueled development with high challenges to mitigation and low challenges to adaptation (*61*). It represents the high end of the range of future pathways with effective radiative forcing of 8.5 W m^{-2} in 2100 (*60*). All CMIP6 historical simulations and future projections used in this study are freely available for research and can be downloaded from https://esgf-data.dkrz.de/search/cmip6-dkrz/.

To evaluate CMIP6 model performance, we compared CMIP6-simulated temperature change with that in EN4 (*37*), which is based on observations and can be downloaded from www.metoffice.gov.uk/hadobs/en4/. CMIP6-simulated ocean heat transport and sea surface heat flux are also compared with the results from the Ocean Re-Analysis System 5 (ORAS5) dataset (*62*), which can be downloaded from www.cen.uni-hamburg.de/en/icdc/data/ocean/easy-init-ocean/ecmwf-oras5.html. The ocean warming and changes in ocean heat transport and sea surface heat flux shown by EN4 and ORAS5 are largely reproduced in the CMIP6 multimodel means, although there are some model biases (Figs. 1 to 4).

CMIP6 models have large intermodel spreads (Figs. 1, 3, and 4), which can be attributed to both different natural variabilities in model simulations and model uncertainties. We used the CESM large ensemble dataset (from www.cesm.ucar.edu/projects/community-projects/LENS/data-sets.html) (*63*) to study the main reason. The ocean temperatures and the warming rates in the Arctic and global oceans have much smaller spreads among 40 CESM ensemble members (fig. S10) than the intermodel spreads among the 20 CMIP6 climate model simulations (Fig. 1). This implies that the large intermodel spreads in CMIP6 models should be mainly caused by climate model uncertainties, and it is sufficient to use one realization from each model in this study. Despite model uncertainties, all models consistently show that ocean heat transport is the main driver for the Arctic Ocean warming (fig. S5).

AOA factor

AOA factor is defined as the ratio of the forced instantaneous warming rate of the Arctic Ocean to that of the global ocean. The warming rate is calculated on the basis of the ensemble empirical mode decomposition (EEMD) (*64*, *65*). EEMD is a noise-assisted data analysis method based on EMD to avoid mode mixing (*65*). In EEMD, a time series of temperature $T(t)$ is decomposed into a number of amplitude-frequency–modulated oscillatory components $C_j(t)$, and a residual $R_n(t)$ after n number of $C_j(t)$ are extracted, with $R_n(t)$ either monotonic or containing only one extremum such that no additional modulated oscillatory components can be extracted (*66*)

$$T(t) = \sum_{j=1}^{n} C_j(t) + R_n(t) \quad (1)$$

where the oscillatory components $C_j(t)$ represent different natural variabilities, while the residual $R_n(t)$ can be considered as the forced change. The decomposition stops when $R_n(t)$ contains at most one extremum, where the total number of $C_j(t)$ (n) is close to $(\log_2 N) - 1$ with N the number of total data points. The forced instantaneous warming rate is the time derivative of the residual, which does not contain influences from natural climate variabilities. The warming rate and AOA factors were calculated for each model separately before computing their multimodel means.

To determine the ToE of AOA, we used the 40 CESM ensemble members mentioned above. The ToE of AOA is defined as the time after which the decadal Arctic Ocean warming is always larger than that of the global ocean mean, a criterion also used to define the ToE of AA (*67*). The ToE was calculated for each ensemble member separately before calculating the ensemble mean (fig. S2). As we have calculated the AOA factor for the CMIP6 models after removing the natural variabilities using EEMD, the time after which the AOA factor remains larger than one also can be considered as the ToE. The consistency of the ToE between the CESM ensemble members and the CMIP6 models helped us determine that the AOA has already emerged in the historical period.

Ocean heat transport

In the Arctic Ocean heat budget analysis, ocean heat transport through each Arctic Ocean gateway (i.e., the Bering Strait, BSO, Fram Strait, and Davis Strait; fig. S3) was calculated using monthly seawater potential temperature and ocean velocity as follows

$$\mathrm{OHT}(v, T) = \rho_o c_p \int_{-H(\lambda)}^{0} \int_{\lambda_1(z)}^{\lambda_2(z)} v(T - T_{\mathrm{ref}})\, d\lambda dz \quad (2)$$

where ρ_o is seawater density, c_p is the specific heat capacity of seawater, v is ocean velocity perpendicular to the section of each gateway, T is the potential temperature in each section, T_{ref} is the reference temperature set to be 0°C in this study, H is water depth, and λ is the distance along the gateway transect. The density and heat capacity–dependent parts of the heat transport changes are ignored in this study because they are treated as constants in our calculations.

We calculated the gateway heat transport along the zigzag grid lines on the native model grids to largely guarantee heat conservation and avoid ambiguities associated with a regridded land/sea mask (*68*). The calculated ocean heat transport can basically ensure the heat conservation as indicated by the fact that the Arctic Ocean temperature anomaly calculated from the sum of the gateway heat transport and ocean surface heat flux is very close to the temperature anomaly directly obtained from the model output (fig. S4).

Decomposition of ocean heat transport

To investigate the changes of ocean heat transport, the ocean heat transport was decomposed as follows (*44*)

$$\mathrm{OHT}(v,T) = \mathrm{OHT}(\overline{v},\overline{T}) + \mathrm{OHT}(\overline{v},T') + \mathrm{OHT}(v',\overline{T}) + \mathrm{OHT}(v',T') \quad (3)$$

where the overbar indicates the climatology and the prime indicates the anomalies from the climatology. Thus, the ocean heat transport anomaly $\mathrm{OHT}_{\mathrm{anomaly}}(v,T) = \mathrm{OHT}(v,T) - \mathrm{OHT}(\overline{v},\overline{T})$ can be decomposed as follows

$$\mathrm{OHT}_{\mathrm{anomaly}}(v,T) = \mathrm{OHT}(\overline{v},T') + \mathrm{OHT}(v',\overline{T}) + \mathrm{OHT}(v',T') \quad (4)$$

where $\mathrm{OHT}(\overline{v},T')$, $\mathrm{OHT}(v',\overline{T})$, and $\mathrm{OHT}(v',T')$ represent the temperature-driven component, velocity-driven component, and the component due to the joint variability of temperature and velocity, respectively. $\mathrm{OHT}(v',T')$ is positive when the velocity and temperature anomalies have the same sign. As shown in fig. S6, this term is not negligible for all the Arctic gateways.

Sea surface heat flux

In this study, the sea surface heat flux is the net heat flux across the surface boundary of the liquid ocean and available directly from the model data repository. It is the sum of the net flux of longwave radiation, net flux of shortwave radiation, sensible heat flux, latent heat flux, ice-ocean heat flux, and internal energy in water entering and leaving the ocean.

Halocline base depth and surface mixed layer depth

The Arctic halocline layer is an important insulator between the AW layer and the surface mixed layer. To study the effect of Arctic Ocean warming on the halocline layer, the halocline base depth is defined as the depth where the ratio of the density gradient due to temperature to the density gradient due to salinity equals 0.05 (*49*), that is

$$R_\rho = (\alpha\partial\theta/\partial z)/(\beta\partial S/\partial z) = 0.05 \quad (5)$$

where α, β, θ, and S are the thermal expansion coefficient, haline contraction coefficient, potential temperature and salinity, respectively. This depth characterizes the transition from halocline to thermocline (*49*).

Averaged over the Eurasian Basin, the halocline base depth will be shallower than the surface mixed layer depth in most of the years after 2070. In this case, the halocline base depth is not plotted in Fig. 6C. This condition indicates that the surface mixed layer is in direct contact with the thermocline, and the AW layer heat can easily reach ocean surface and sea ice. The mixed layer depth is defined as the depth where the potential density is larger than the surface potential density by 0.1 kg/m^3 (*69*). We calculated the mixed layer depth and halocline base depth at each model grid point first before calculating the basin means and multimodel means.

SUPPLEMENTARY MATERIALS

Supplementary material for this article is available at https://science.org/doi/10.1126/sciadv.abn9755

REFERENCES AND NOTES

1. I. H. Onarheim, T. Eldevik, L. H. Smedsrud, J. C. Stroeve, Seasonal and regional manifestation of Arctic sea ice loss. *J. Climate* **31**, 4917–4932 (2018).
2. J. Stroeve, D. Notz, Changing state of Arctic sea ice across all seasons. *Environ. Res. Lett.* **13**, 103001 (2018).
3. C. Kinnard, C. M. Zdanowicz, D. A. Fisher, E. Isaksson, A. De Vernal, L. G. Thompson, Reconstructed changes in Arctic sea ice over the past 1,450 years. *Nature* **479**, 509–512 (2011).
4. J. Halfar, W. H. Adey, A. Kronz, S. Hetzinger, E. Edinger, W. W. Fitzhugh, Arctic sea-ice decline archived by multicentury annual-resolution record from crustose coralline algal proxy. *Proc. Natl. Acad. Sci. U.S.A.* **110**, 19737–19741 (2013).
5. R. Kwok, D. A. Rothrock, Decline in Arctic sea ice thickness from submarine and ICESat records: 1958-2008. *Geophys. Res. Lett.* **36**, L15501 (2009).
6. J. Maslanik, J. Stroeve, C. Fowler, W. Emery, Distribution and trends in Arctic sea ice age through spring 2011. *Geophys. Res. Lett.* **38**, L13502 (2011).
7. M. Wang, J. E. Overland, A sea ice free summer Arctic within 30 years? *Geophys. Res. Lett.* **36**, L07502 (2009).
8. M. Wang, J. E. Overland, A sea ice free summer Arctic within 30 years: An update from CMIP5 models. *Geophys. Res. Lett.* **39**, L18501 (2012).
9. J. A. Screen, I. Simmonds, The central role of diminishing sea ice in recent Arctic temperature amplification. *Nature* **464**, 1334–1337 (2010).
10. J. Cohen, J. A. Screen, J. C. Furtado, M. Barlow, D. Whittleston, D. Coumou, J. Francis, K. Dethloff, D. Entekhabi, J. Overland, J. Jones, Recent Arctic amplification and extreme mid-latitude weather. *Nat. Geosci.* **7**, 627–637 (2014).
11. J. Cohen, X. Zhang, J. Francis, T. Jung, R. Kwok, J. Overland, T. J. Ballinger, U. S. Bhatt, H. W. Chen, D. Coumou, S. Feldstein, H. Gu, D. Handorf, G. Henderson, M. Ionita, M. Kretschmer, F. Laliberte, S. Lee, H. W. Linderholm, W. Maslowski, Y. Peings, K. Pfeiffer, I. Rigor, T. Semmler, J. Stroeve, P. C. Taylor, S. Vavrus, T. Vihma, S. Wang, M. Wendisch, Y. Wu, J. Yoon, Divergent consensuses on Arctic amplification influence on midlatitude severe winter weather. *Nat. Clim. Change* **10**, 20–29 (2020).
12. R. G. Graversen, T. Mauritsen, M. Tjernström, E. Källén, G. Svensson, Vertical structure of recent Arctic warming. *Nature* **451**, 53–56 (2008).
13. D. M. Smith, J. A. Screen, C. Deser, J. Cohen, J. C. Fyfe, J. García-Serrano, T. Jung, V. Kattsov, D. Matei, R. Msadek, Y. Peings, M. Sigmond, J. Ukita, X. Zhang, The polar amplification model intercomparison project (PAMIP) contribution to CMIP6: Investigating the causes and consequences of polar amplification. *Geosci. Model Dev.* **12**, 1139–1164 (2019).
14. M. F. Stuecker, C. M. Bitz, K. C. Armour, C. Proistosescu, S. M. Kang, S. P. Xie, D. Kim, S. McGregor, W. Zhang, S. Zhao, W. Cai, Y. Dong, F. F. Jin, Polar amplification dominated by local forcing and feedbacks. *Nat. Clim. Chang.* **8**, 1076–1081 (2018).
15. A. Dai, D. Luo, M. Song, J. Liu, Arctic amplification is caused by sea-ice loss under increasing CO_2. *Nat. Commun.* **10**, 121 (2019).
16. F. Pithan, T. Mauritsen, Arctic amplification dominated by temperature feedbacks in contemporary climate models. *Nat. Geosci.* **7**, 181–184 (2014).
17. E. S. Chung, K. J. Ha, A. Timmermann, M. F. Stuecker, T. Bodai, S. K. Lee, Cold-season Arctic amplification driven by Arctic Ocean-mediated seasonal energy transfer. *Earths Future* **9**, e2020EF001898 (2021).
18. Y. Huang, Y. Xia, X. Tan, On the pattern of CO_2 radiative forcing and poleward energy transport. *J. Geophys. Res. Atmos.* **122**, 10578–10593 (2017).
19. E. Beer, I. Eisenman, T. J. W. Wagner, Polar amplification due to enhanced heat flux across the halocline. *Geophys. Res. Lett.* **47**, e2019GL086706 (2020).
20. I. V. Polyakov, G. V. Alekseev, L. A. Timokhov, U. S. Bhatt, R. L. Colony, H. L. Simmons, D. Walsh, J. E. Walsh, V. F. Zakharov, Variability of the intermediate Atlantic water of the Arctic Ocean over the last 100 years. *J. Climate* **17**, 4485–4497 (2004).

21. I. V. Polyakov, A. V. Pnyushkov, L. A. Timokhov, Warming of the intermediate Atlantic water of the Arctic ocean in the 2000S. *J. Climate* **25**, 8362–8370 (2012).
22. M. Korhonen, B. Rudels, M. Marnela, A. Wisotzki, J. Zhao, Time and space variability of freshwater content, heat content and seasonal ice melt in the Arctic Ocean from 1991 to 2011. *Ocean Sci.* **9**, 1015–1055 (2013).
23. S. Lind, R. B. Ingvaldsen, T. Furevik, Arctic warming hotspot in the northern Barents Sea linked to declining sea-ice import. *Nat. Clim. Chang.* **8**, 634–639 (2018).
24. Ø. Skagseth, T. Eldevik, M. Årthun, H. Asbjørnsen, V. S. Lien, L. H. Smedsrud, Reduced efficiency of the Barents Sea cooling machine. *Nat. Clim. Chang.* **10**, 661–666 (2020).
25. S. Watelet, Ø. Skagseth, V. S. Lien, H. Sagen, Ø. Østensen, V. Ivshin, J. M. Beckers, A volumetric census of the Barents Sea in a changing climate. *Earth Syst. Sci. Data.* **12**, 2447–2457 (2020).
26. Z. Li, Q. Ding, M. Steele, A. Schweiger, Recent upper Arctic Ocean warming expedited by summertime atmospheric processes. *Nat. Commun.* **13**, 362 (2022).
27. I. V. Polyakov, A. V. Pnyushkov, M. B. Alkire, I. M. Ashik, T. M. Baumann, E. C. Carmack, I. Goszczko, J. Guthrie, V. V. Ivanov, T. Kanzow, R. Krishfield, R. Kwok, A. Sundfjord, J. Morison, R. Rember, A. Yulin, Greater role for Atlantic inflows on sea-ice loss in the Eurasian Basin of the Arctic Ocean. *Science* **356**, 285–291 (2017).
28. I. V. Polyakov, M. B. Alkire, B. A. Bluhm, K. A. Brown, E. C. Carmack, M. Chierici, S. L. Danielson, I. Ellingsen, E. A. Ershova, K. Gårdfeldt, R. B. Ingvaldsen, A. V. Pnyushkov, D. Slagstad, P. Wassmann, Borealization of the Arctic Ocean in response to anomalous advection from sub-Arctic seas. *Front. Mar. Sci.* **7**, 491 (2020).
29. M. Årthun, T. Eldevik, L. H. Smedsrud, Ø. Skagseth, R. B. Ingvaldsen, Quantifying the influence of atlantic heat on barents sea ice variability and retreat. *J. Climate* **25**, 4736–4743 (2012).
30. R. A. Woodgate, Increases in the Pacific inflow to the Arctic from 1990 to 2015, and insights into seasonal trends and driving mechanisms from year-round Bering Strait mooring data. *Prog. Oceanogr.* **160**, 124–154 (2018).
31. M. L. Timmermans, J. Toole, R. Krishfield, Warming of the interior Arctic Ocean linked to sea ice losses at the basin margins. *Sci. Adv.* **4**, eaat6773 (2018).
32. H. Asbjørnsen, M. Årthun, Ø. Skagseth, T. Eldevik, Mechanisms underlying recent Arctic atlantification. *Geophys. Res. Lett.* **47**, e2020GL088036 (2020).
33. Q. Shu, Q. Wang, Z. Song, F. Qiao, The poleward enhanced Arctic Ocean cooling machine in a warming climate. *Nat. Commun.* **12**, 2966 (2021).
34. M. Årthun, T. Eldevik, L. H. Smedsrud, The role of Atlantic heat transport in future Arctic winter sea ice loss. *J. Climate* **32**, 3327–3341 (2019).
35. J. A. Screen, I. Simmonds, Increasing fall-winter energy loss from the Arctic Ocean and its role in Arctic temperature amplification. *Geophys. Res. Lett.* **37**, L16707 (2010).
36. M. Previdi, K. L. Smith, L. M. Polvani, Arctic amplification of climate change: A review of underlying mechanisms. *Environ. Res. Lett.* **16**, 093003 (2021).
37. S. A. Good, M. J. Martin, N. A. Rayner, EN4: Quality controlled ocean temperature and salinity profiles and monthly objective analyses with uncertainty estimates. *J. Geophys. Res. Oceans* **118**, 6704–6716 (2013).
38. T. W. N. Haine, T. Martin, The Arctic-Subarctic sea ice system is entering a seasonal regime: Implications for future Arctic amplification. *Sci. Rep.* **7**, 4618 (2017).
39. C. Burgard, D. Notz, Drivers of Arctic Ocean warming in CMIP5 models. *Geophys. Res. Lett.* **44**, 4263–4271 (2017).
40. M. Ilicak, H. Drange, Q. Wang, R. Gerdes, Y. Aksenov, D. Bailey, M. Bentsen, A. Biastoch, A. Bozec, C. Böning, C. Cassou, E. Chassignet, A. C. Coward, B. Curry, G. Danabasoglu, S. Danilov, E. Fernandez, P. G. Fogli, Y. Fujii, S. M. Griffies, D. Iovino, A. Jahn, T. Jung, W. G. Large, C. Lee, C. Lique, J. Lu, S. Masina, A. J. George Nurser, C. Roth, D. Salas y Mélia, B. L. Samuels, P. Spence, H. Tsujino, S. Valcke, A. Voldoire, X. Wang, S. G. Yeager, An assessment of the Arctic Ocean in a suite of interannual CORE-II simulations. Part III: Hydrography and fluxes. *Ocean Model.* **100**, 141–161 (2016).
41. Q. Wang, X. Wang, C. Wekerle, S. Danilov, T. Jung, N. Koldunov, S. Lind, D. Sein, Q. Shu, D. Sidorenko, Ocean heat transport into the barents sea: Distinct controls on the upward trend and interannual variability. *Geophys. Res. Lett.* **46**, 13180–13190 (2019).
42. Q. Wang, C. Wekerle, X. Wang, S. Danilov, N. Koldunov, D. Sein, D. Sidorenko, W. J. von Appen, T. Jung, Intensification of the atlantic water supply to the Arctic Ocean through fram strait induced by Arctic sea ice decline. *Geophys. Res. Lett.* **47**, e2019GL086682 (2020).
43. R. A. Woodgate, C. Peralta-Ferriz, Warming and freshening of the Pacific inflow to the Arctic From 1990-2019 implying dramatic shoaling in Pacific winter water ventilation of the Arctic water column. *Geophys. Res. Lett.* **48**, e2021GL092528 (2021).
44. T. Tsubouchi, K. Våge, B. Hansen, K. M. H. Larsen, S. Østerhus, C. Johnson, S. Jónsson, H. Valdimarsson, Increased ocean heat transport into the Nordic Seas and Arctic Ocean over the period 1993–2016. *Nat. Clim. Chang.* **11**, 21–26 (2021).
45. J. Dörr, M. Årthun, T. Eldevik, E. Madonna, Mechanisms of regional winter sea-ice variability in a warming arctic. *J. Climate* **34**, 8635–8653 (2021).
46. Q. Shu, F. Qiao, Z. Song, J. Zhao, X. Li, Projected freshening of the Arctic Ocean in the 21st century. *J. Geophys. Res. Oceans* **123**, 9232–9244 (2018).
47. N. Khosravi, Q. Wang, N. Koldunov, C. Hinrichs, T. Semmler, S. Danilov, T. Jung, The Arctic Ocean in CMIP6 Models: Biases and projected changes in temperature and salinity. *Earths Future* **10**, e2021ef002282 (2022).
48. C. M. Bitz, G. H. Roe, A mechanism for the high rate of sea ice thinning in the Arctic Ocean. *J. Climate* **17**, 3623–3632 (2004).
49. P. Bourgain, J. C. Gascard, The Arctic Ocean halocline and its interannual variability from 1997 to 2008. *Deep Sea Res. 1 Oceanogr. Res. Pap.* **58**, 745–756 (2011).
50. I. V. Polyakov, T. P. Rippeth, I. Fer, M. B. Alkire, T. M. Baumann, E. C. Carmack, R. Ingvaldsen, V. V. Ivanov, M. Janout, S. Lind, L. Padman, A. V. Pnyushkov, R. Rember, Weakening of cold halocline layer exposes sea ice to oceanic heat in the eastern arctic ocean. *J. Climate* **33**, 8107–8123 (2020).
51. J. R. Shi, S. P. Xie, L. D. Talley, Evolving relative importance of the Southern Ocean and North Atlantic in anthropogenic ocean heat uptake. *J. Climate* **31**, 7459–7479 (2018).
52. D. Oldenburg, K. C. Armour, L. A. Thompson, C. M. Bitz, Distinct mechanisms of ocean heat transport into the Arctic under internal variability and climate change. *Geophys. Res. Lett.* **45**, 7692–7700 (2018).
53. A. Nummelin, C. Li, P. J. Hezel, Connecting ocean heat transport changes from the midlatitudes to the Arctic Ocean. *Geophys. Res. Lett.* **44**, 1899–1908 (2017).
54. L. Oziel, A. Baudena, M. Ardyna, P. Massicotte, A. Randelhoff, J. B. Sallée, R. B. Ingvaldsen, E. Devred, M. Babin, Faster Atlantic currents drive poleward expansion of temperate phytoplankton in the Arctic Ocean. *Nat. Commun.* **11**, 1705 (2020).
55. S. L. Danielson, O. Ahkinga, C. Ashjian, E. Basyuk, L. W. Cooper, L. Eisner, E. Farley, K. B. Iken, J. M. Grebmeier, L. Juranek, G. Khen, S. R. Jayne, T. Kikuchi, C. Ladd, K. Lu, R. M. McCabe, G. W. K. Moore, S. Nishino, F. Ozenna, R. S. Pickart, I. Polyakov, P. J. Stabeno, R. Thoman, W. J. Williams, K. Wood, T. J. Weingartner, Manifestation and consequences of warming and altered heat fluxes over the Bering and Chukchi Sea continental shelves. *Deep Sea Res. 2 Top. Stud. Oceanogr.* **177**, 104781 (2020).
56. S. Hu, S. P. Xie, S. M. Kang, Global warming pattern formation: The role of ocean heat uptake. *J. Climate* **35**, 1885–1899 (2022).
57. M. Karcher, A. Beszczynska-Möller, F. Kauker, R. Gerdes, S. Heyen, B. Rudels, U. Schauer, Arctic Ocean warming and its consequences for the Denmark Strait overflow. *J. Geophys. Res. Oceans* **116**, e2010JC006265 (2011).
58. H. Bailey, A. Hubbard, E. S. Klein, K. R. Mustonen, P. D. Akers, H. Marttila, J. M. Welker, Arctic sea-ice loss fuels extreme European snowfall. *Nat. Geosci.* **14**, 283–288 (2021).
59. F. Li, X. Wan, H. Wang, Y. J. Orsolini, Z. Cong, Y. Gao, S. Kang, Arctic sea-ice loss intensifies aerosol transport to the Tibetan Plateau. *Nat. Clim. Chang.* **10**, 1037–1044 (2020).
60. B. C. O'Neill, C. Tebaldi, D. P. Van Vuuren, V. Eyring, P. Friedlingstein, G. Hurtt, R. Knutti, E. Kriegler, J. F. Lamarque, J. Lowe, G. A. Meehl, R. Moss, K. Riahi, B. M. Sanderson, The Scenario Model Intercomparison Project (ScenarioMIP) for CMIP6. *Geosci. Model Dev.* **9**, 3461–3482 (2016).
61. K. Riahi, D. P. van Vuuren, E. Kriegler, J. Edmonds, B. C. O'Neill, S. Fujimori, N. Bauer, K. Calvin, R. Dellink, O. Fricko, W. Lutz, A. Popp, J. C. Cuaresma, S. KC, M. Leimbach, L. Jiang, T. Kram, S. Rao, J. Emmerling, K. Ebi, T. Hasegawa, P. Havlik, F. Humpenöder, L. A. Da Silva, S. Smith, E. Stehfest, V. Bosetti, J. Eom, D. Gernaat, T. Masui, J. Rogelj, J. Strefler, L. Drouet, V. Krey, G. Luderer, M. Harmsen, K. Takahashi, L. Baumstark, J. C. Doelman, M. Kainuma, Z. Klimont, G. Marangoni, H. Lotze-Campen, M. Obersteiner, A. Tabeau, M. Tavoni, The shared socioeconomic pathways and their energy, land use, and greenhouse gas emissions implications: An overview. *Glob. Environ. Chang.* **42**, 153–168 (2017).
62. H. Zuo, M. A. Balmaseda, S. Tietsche, K. Mogensen, M. Mayer, The ECMWF operational ensemble reanalysis-analysis system for ocean and sea ice: A description of the system and assessment. *Ocean Sci.* **15**, 779–808 (2019).
63. J. E. Kay, C. Deser, A. Phillips, A. Mai, C. Hannay, G. Strand, J. M. Arblaster, S. C. Bates, G. Danabasoglu, J. Edwards, M. Holland, P. Kushner, J. F. Lamarque, D. Lawrence, K. Lindsay, A. Middleton, E. Munoz, R. Neale, K. Oleson, L. Polvani, M. Vertenstein, The community earth system model (CESM) large ensemble project: A community resource for studying climate change in the presence of internal climate variability. *Bull. Am. Meteorol. Soc.* **96**, 1333–1349 (2015).
64. N. E. Huang, Z. Shen, S. R. Long, M. C. Wu, H. H. Snin, Q. Zheng, N. C. Yen, C. C. Tung, H. H. Liu, The empirical mode decomposition and the Hilbert spectrum for nonlinear and non-stationary time series analysis. *Proc. R. Soc. A Math. Phys. Eng. Sci.* **454**, 903–995 (1998).
65. Z. Wu, N. E. Huang, Ensemble empirical mode decomposition: A noise-assisted data analysis method. *Adv. Adapt. Data Anal.* **1**, 1–41 (2009).
66. Z. Wu, N. E. Huang, S. R. Long, C. K. Peng, On the trend, detrending, and variability of nonlinear and nonstationary time series. *Proc. Natl. Acad. Sci. U.S.A.* **104**, 14889–14894 (2007).
67. M. M. Holland, L. Landrum, The emergence and transient nature of Arctic amplification in coupled climate models. *Front. Earth Sci.* **9**, 719024 (2021).
68. S. M. Griffies, G. Danabasoglu, P. J. Durack, A. J. Adcroft, V. Balaji, C. W. Böning, E. P. Chassignet, E. Curchitser, J. Deshayes, H. Drange, B. Fox-Kemper, P. J. Gleckler,

J. M. Gregory, H. Haak, R. W. Hallberg, P. Heimbach, H. T. Hewitt, D. M. Holland, T. Ilyina, J. H. Jungclaus, Y. Komuro, J. P. Krasting, W. G. Large, S. J. Marsland, S. Masina, T. J. McDougall, A. J. George Nurser, J. C. Orr, A. Pirani, F. Qiao, R. J. Stouffer, K. E. Taylor, A. M. Treguier, H. Tsujino, P. Uotila, M. Valdivieso, Q. Wang, M. Winton, S. G. Yeager, OMIP contribution to CMIP6: Experimental and diagnostic protocol for the physical component of the Ocean Model Intercomparison Project. *Geosci. Model Dev.* **9**, 3231–3296 (2016).

69. C. Peralta-Ferriz, R. A. Woodgate, Seasonal and interannual variability of pan-Arctic surface mixed layer properties from 1979 to 2012 from hydrographic data, and the dominance of stratification for multiyear mixed layer depth shoaling. *Prog. Oceanogr.* **134**, 19–53 (2015).

Acknowledgments

Funding: This work was supported by the Chinese Natural Science Foundation grants 41821004, 41941012, and 42022042; German Helmholtz Climate Initiative REKLIM (Regional Climate Change); EPICA project in the research theme MARE: N - Polarforschung/MOSAiC funded by the German Federal Ministry for Education and Research grant 03F0889A; and Research Council of Norway project Nansen Legacy grant 276730. **Author contributions:** Conceptualization: Q.S., Q.W., and F.Q. Methodology: S.W., M.Z., and Z.S. Investigation: Q.S., Q.W., S.W., M.Z. Visualization: Q.S. and Q.W. Supervision: Z.S. and F.Q. Writing—original draft: Q.S., Q.W., and M.Å. Writing—review and editing: Q.S., Q.W., M.Å., and F.Q. **Competing interests:** The authors declare that they have no competing interests. **Data and materials availability:** All data needed to evaluate the conclusions in the paper are present in the paper and/or the Supplementary Materials. All the data used in this research are freely available to the public for research and can be downloaded through the links detailed in Materials and Methods. The EMD package used for AOA factor calculation is available in MATLAB version 2018a and later versions. The MATLAB package used for calculating transports through the four Arctic Ocean gateways is available at https://zenodo.org/record/6630376#.YqLv2XZBzFg. The codes used for data processing and visualization can be found at https://figshare.com/articles/dataset/Arctic_Ocean_Amplification_in_a_warming_climate_in_CMIP6_models/19767652.

Submitted 5 January 2022
Accepted 5 June 2022
Published 27 July 2022
10.1126/sciadv.abn9755

ScienceAdvances

Arctic Ocean Amplification in a warming climate in CMIP6 models

Qi Shu, Qiang Wang, Marius Årthun, Shizhu Wang, Zhenya Song, Min Zhang, and Fangli Qiao

Sci. Adv. **8** (30), eabn9755. DOI: 10.1126/sciadv.abn9755

Science Advances (ISSN 2375-2548) is published by the American Association for the Advancement of Science. 1200 New York Avenue NW, Washington, DC 20005. The title *Science Advances* is a registered trademark of AAAS.